

Observation of Shapiro steps in an ultracold atomic Josephson junction

Erik Bernhart¹ Marvin Röhrle¹, Vijay Pal Singh², Ludwig Mathey^{3,4}, Luigi Amico,^{2,5,6,*} and Herwig Ott^{1,†}

¹*Department of Physics and Research Center OPTIMAS,
Rheinland-Pfälzische Technische Universität Kaiserslautern-Landau, 67663 Kaiserslautern, Germany*

²*Quantum Research Centre, Technology Innovation Institute, Abu Dhabi, UAE*

³*Zentrum für Optische Quantentechnologien and Institut für Quantenphysik, Universität Hamburg, 22761 Hamburg, Germany*

⁴*The Hamburg Centre for Ultrafast Imaging, Luruper Chaussee 149, Hamburg 22761, Germany*

⁵*Dipartimento di Fisica e Astronomia, Università di Catania, Via S. Sofia 64, 95123 Catania, Italy*

⁶*INFN-Sezione di Catania, Via S. Sofia 64, 95127 Catania, Italy*

(Dated: September 6, 2024)

The current-voltage characteristic of a driven superconducting Josephson junction displays discrete steps. This phenomenon, discovered by Sydney Shapiro, forms today's voltage standard. Here, we report the observation of Shapiro steps in a driven Josephson junction in a gas of ultracold atoms. We demonstrate that the steps exhibit universal features, and provide key insight into the microscopic dissipative dynamics that we directly observe in the experiment. Most importantly, the steps are directly connected to phonon emission and soliton nucleation. The experimental results are underpinned by extensive numerical simulations based on classical-field dynamics and represent the transfer of the voltage standard to the realm of ultracold quantum gases.

INTRODUCTION

The Josephson effect is one of the most fundamental phenomena in quantum science and technology: originally discovered for superconductors, the effect features a dissipation-less electrical current through a tunnel barrier by virtue of the phase difference of the traversing Cooper pairs' wave function. Above a critical value of the current, a finite voltage occurs across the junction as a result of the formation of superconducting quasi-particles [1]. The Josephson effect and Josephson junctions have played a prominent role for understanding the notion of macroscopic quantum coherence, which led to important technological applications such as SQUIDs [2–6] and are the core units of superconducting qubits [7–10]. If an additional microwave field is applied across the Josephson junction, a staircase current-voltage characteristic emerges, referred to as Shapiro steps [11]. The origin of this effect is photon-assisted tunneling of Cooper pairs through the junction [5]. Since the height of the steps depends only on the frequency of the microwave radiation, Planck's constant, and the electric charge, Shapiro steps are nowadays used as the voltage standard - see e.g. [12]. Shapiro steps in superfluid ^3He have been investigated in Ref. [13].

The Josephson effect can also be observed in ultracold quantum gases [14]. On the one hand, this enables the fabrication of atomtronic circuits, which have developed into their own field of research in recent years [15–17]. On the other hand, the high degree of control and flexibility over ultracold quantum gases provides unprecedented access to the microscopic physics underlying the system. In particular, Josephson physics has been recently implemented and extensively studied in ultracold atomic systems, both theoretically [4, 18, 20–22] as well as experimentally in bosonic [14, 23–25] and fermionic

[5, 27] systems. In implementations with ultracold atoms, the Josephson current-phase relation is realized by moving the barrier through an ultracold gas which is otherwise at rest [2, 29]. Shapiro steps in ultracold gases are predicted to appear if the linear translation of the barrier (corresponding to a dc particle current) is combined with a periodic modulation of the position of the barrier (corresponding to an ac particle current), thus emulating the external microwave radiation of the superconducting Josephson junction [12].

Here, we demonstrate the emergence of Shapiro steps at an atomic Josephson junction and quantify their global and local properties. The steps occur in the chemical potential difference, in conjunction with a density imbalance across the junction. We confirm that the step heights in the chemical potential difference $\Delta\mu$ are quantized by the external driving frequency f_m , i.e., $\Delta\mu = nhf_m$, where n is the step index and h is Planck's constant. By spatially resolving the atomic density, we study the microscopic dynamics and observe the propagation of phonons and quasi-particles emerging from the barrier, which we identify as solitons. This paves the way for studying the microscopic dissipative dynamics of Shapiro steps and other related Josephson transport effects. Furthermore, since the magnitude of the step height relates the chemical potential difference to a tunable frequency, and since the density imbalance across the barrier is directly measurable, our results suggest an additional insight into the equation of state of strongly correlated superfluids, thus advancing the study of superfluids with a novel approach.

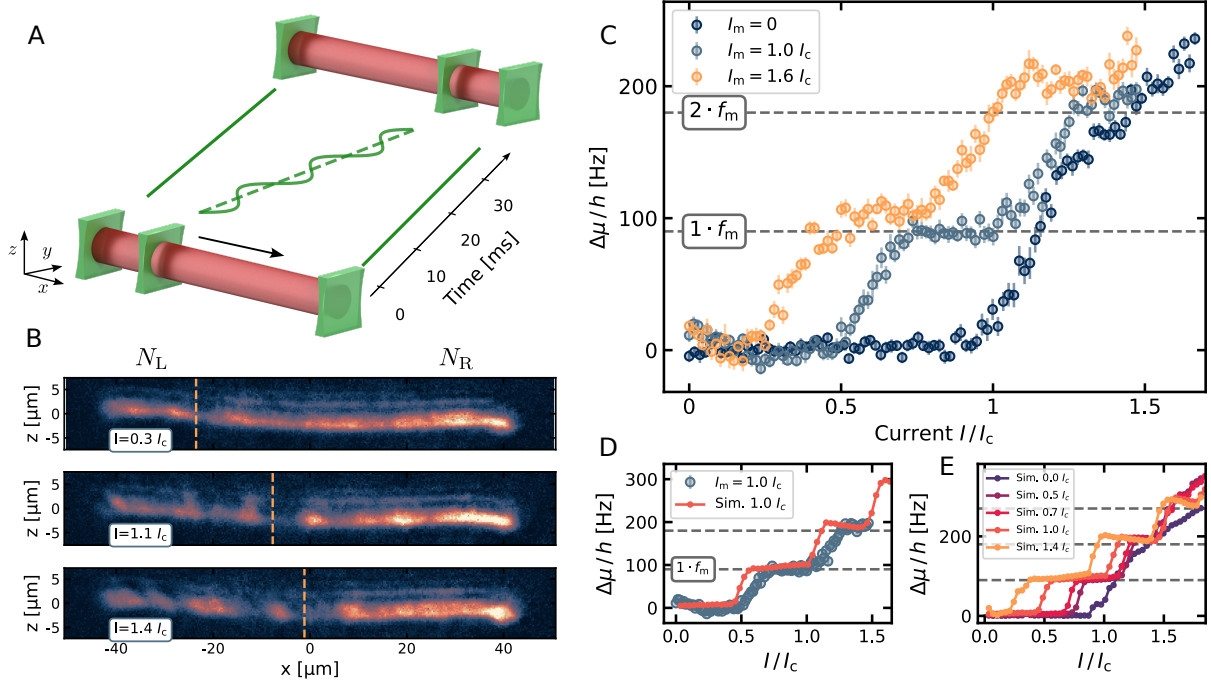


FIG. 1. **Shapiro steps in an ultracold atomic Josephson junction.** (A) The system consists of a cylindrically shaped superfluid which is split by a movable optical barrier creating a weak link. The barrier as well as the two confining end-caps are realized with tightly focused laser beams. In the measurement protocol, the barrier is moved linearly (dc particle current) through the superfluid with an additional harmonic modulation (ac particle current), which is sketched in the figure. (B) At the end of the protocol, a real space absorption image of the atomic cloud is taken, using matter wave imaging [3, 32]. From the atom number imbalance between the two superfluids, their chemical potential difference is derived. The pictures are taken with a modulation current $I_m = 0.8 I_c$. The position of the barrier is marked as a dashed orange line. (C) Measured Shapiro steps for $f_m = 90$ Hz, and different modulation amplitudes I_m . The horizontal lines indicate the ideal Shapiro step height, given by Eq. 2. Every data point is the average of about 25 measurement runs, the vertical bars indicate the error of the mean. (D) Comparison between experiment and classical-field simulation. (E) Simulations of the system at $T = 35$ nK and different I_m .

EXPERIMENTAL SYSTEM

The experimental setup and the Shapiro protocol are sketched in Fig. 1. We prepare a ^{87}Rb Bose-Einstein condensate in an elongated optical dipole trap. The condensate has a tube-like cylindrical geometry with harmonic transverse confinement, see Fig. 1 A. The chemical potential is $\mu = h \times 1900 \text{ s}^{-1}$. A movable repulsive barrier with height $V_B = 0.45 \times \mu$ separates the condensate into two parts and thus realizes a weak link [32]. We probe the system by absorption imaging. To achieve a high accuracy, we perform a matter wave imaging scheme [3] in order to reduce the optical density [32].

We implement the dc and ac driving protocol following the proposal in Ref. [12]. To this end, we move the barrier with constant velocity v and an additional periodic modulation,

$$x(t) = vt + x_m \sin(2\pi f_m t), \quad (1)$$

where x_m is the modulation amplitude, and f_m the modulation frequency. We fix the driving time to 33 ms,

which means that the final position of the barrier depends on v . At the end, we measure the atom number imbalance $z = (N_R - N_L)/N$, where N is the total atom number and N_L (N_R) is the atom number on the left (right) hand side of the barrier. As a reference z_{ref} , we also measure the corresponding imbalance without the barrier. Using a simulation of the Gross-Pitaevskii equation we map $\Delta z = z - z_{\text{ref}}$ to the chemical potential difference $\Delta\mu$ [32]. The barrier motion induces an atomic current relative to the barrier of value I , with $I = vI_c/v_c$, where I_c is the critical current and v_c is the critical velocity [32]. The external current then reads $I_{\text{ext}} = I + I_{\text{ac}} = I + I_m \sin(2\pi f_m t)$, with the bias current I and the modulation current I_m . The parameters which we modify in our protocol are I , I_m and f_m . In Fig. 1 C we show the measurements of the current-chemical potential characteristics that are obtained without and with ac driving. From the undriven response we characterize the critical velocity and the critical current of the Josephson junction [32]. For the periodically driven case, the system features plateaus of constant chemical potential difference occurring at integer multiple of the

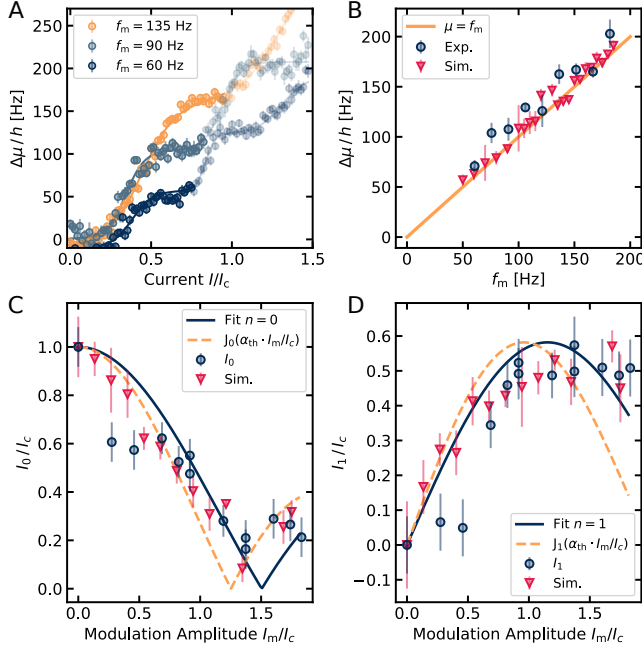


FIG. 2. **Characteristics of the Shapiro steps.** (A) Dependence of the step height on the modulation frequency f_m , where the step height is determined using sigmoid fits (continuous lines). (B) Measurements of the step height (dots) are compared to the numerical simulations (triangles) and the prediction $\Delta\mu/h = f_m$ (continuous line). (C and D) Measurements (dots) and simulation (triangles) of zeroth and first step widths (I_0 and I_1) for varying I_m/I_c . The solid blue lines are a fit to the experimental data, and the dashed orange lines indicate the theoretical prediction, following Eq. 3.

driving frequency. Thereby, the steps occur at lower I for stronger I_m . We model our system with extensive classical-field simulations [32], which capture the feature of our driven Josephson junction well, see Fig. 1 D, E.

In a superconducting Josephson junction where the Shapiro steps arise from photon-assisted tunneling of the Cooper pairs [33], the voltage V_n of the n -th Shapiro step is directly given by the energy quantization, i.e., $V_n = n\Phi_0 f_m = n f_m h/(2e)$, where Φ_0 is the flux quantum and e the elementary charge [5, 34]. For our neutral atom implementation this results in the quantization condition

$$\Delta\mu = nh f_m. \quad (2)$$

To confirm this fundamental relation we vary f_m and determine the height $\Delta\mu$ of the first step, see Fig. 2 A. For the modulation frequencies explored here, we indeed find the behavior $\Delta\mu = h f_m$, see Fig. 2 B. This result establishes the transfer of the voltage standard to the realm of ultracold quantum gases [35]. This is particularly useful in situations, where the relation between the atomic density and the chemical potential is not known, as the protocol allows for the generation of a predetermined chemical potential difference.

Next, we analyze the width of the Shapiro steps by varying the modulation amplitude I_m/I_c at a fixed modulation frequency of $f_m = 90$ Hz [32]. In Fig. 2 C, D, the widths of the zeroth and first steps display a Bessel-function behavior as a function of I_m/I_c , which is in agreement with the results of numerical simulations [32]. To support this observation we use the analytical prediction of an ac voltage driven Josephson junction, which yields the step width $I_n = I_c |J_n(V_m/V_n)|$, where J_n is the Bessel function of the n -th order and V_m the modulation voltage [5, 36]. For an ac current driven junction this can be mathematically transformed into

$$I_n = I_c \left| J_n \left(\alpha_{th} \frac{I_m}{I_c} \right) \right|, \quad (3)$$

with $\alpha_{th} = RI_c/f_m$. The resistance R and I_c are determined independently, such that there is no free fitting parameter [32]. In Fig. 2 C, D the results of Eq. 3 support the overall trend of our measurements and simulations.

MICROSCOPIC DYNAMICS

In contrast to solid-state physics the time and length scales in quantum gas experiments are much larger, such that the *in situ* study of excitations, quasi-particles and related microscopic phenomena becomes possible. To do so, we follow the time evolution of the real space atomic density. Using only a constant barrier velocity, i.e., no ac particle current, we measure the dc and ac Josephson regime, see Fig. 3 A. Below the critical current no imbalance is created and only a single phononic density wave is emitted from the initial acceleration of the barrier (I and II). The group velocity of the emitted phonons coincides with a reference measurement, where a single perturbation creates a phonon wave packet [32]. In the ac Josephson regime above the critical current, atoms are pushed away by the barrier and a density depletion remains in its wake (III).

In the Shapiro regime instead, we see that the phase dynamics is characterized by two distinct collective excitations: phonons and localized density depletions (see Fig. 3 B and C). Phonons are emitted at distinct times in both directions due to the oscillatory motion of the barrier. This is particularly visible on the zeroth plateau (I). Increasing the constant current I beyond the zeroth plateau yields a chemical potential difference and atom number imbalance; this phenomenon is characterized by the formation of 'depletion waves' that move backwards compared to the barrier motion (blue lines propagating to the left in II and III). These excitations are observed to have a smaller group velocity, i.e., a steeper slope and, by using the phase information of the simulation in Fig. 4 A, we can conclude that such defects are accompanied by well resolved phase slippages with a phase jump of less

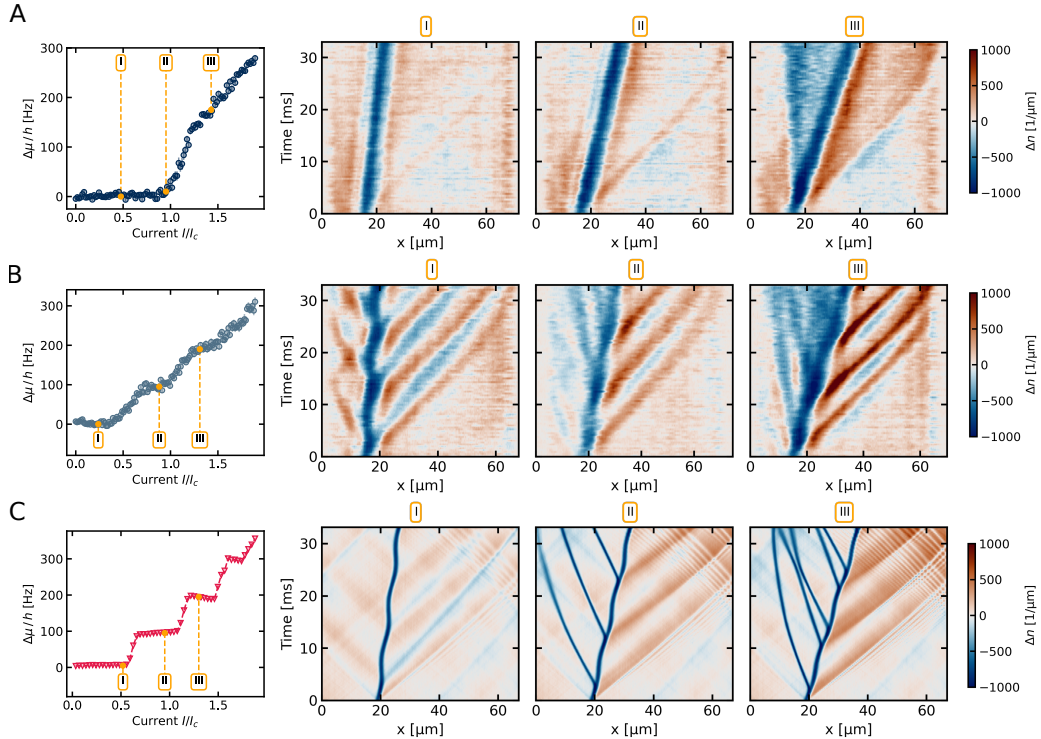


FIG. 3. Microscopic system dynamics. Time evolution of the atomic density in the experiment (A, B) and in the simulation (C). **(A)** Constant barrier velocity. We show the time evolution for three different currents, indicated in the $I - \Delta\mu$ plot on the left. **(B)** Constant plus periodically modulated barrier velocity (Shapiro protocol), where $I_m = 0.8I_c$ and $f_m = 90$ Hz. **(C)** Classical-field simulations of the driven junction, with $I_m = 0.8I_c$ and $f_m = 90$ Hz. Each horizontal line in the images corresponds to a transversely integrated absorption image, which are stacked together. The color code indicates the relative change of the line density with respect to a reference image without barrier.

than π at the density minimum. Therefore we identify these excitations as grey solitons. These solitons are responsible for most of the reduction in density, ultimately causing the particle imbalance across the junction- see Fig. 4 B and C. Specifically, the simulation suggests that for the n -th plateau n solitons are on-average emitted backwards during one driving cycle, see panels II and III of Fig. 3 C and [32]. This creates the reduced density in the wake of the moving barrier, and therefore gives rise to the resistive regime. On the other hand, being also defects of the phase field, they play a similar role as quasi-particles of the driven superconducting Josephson junctions: as single-particle excitations are responsible for the resistive transport and for the actual phase dynamics across the superconducting junction, soliton emission provides the specific mechanism for the evolution of the phase coherence in our system, thus allowing for phase coherent dynamics even in presence of dissipation.

In this sense, soliton emission in our system plays a similar role to that of single-particle excitations in superconducting Josephson junctions. This statement is corroborated by the fact that the rate of emitted solitons indeed displays a step-like behavior in close parallel with the staircase displayed by the chemical potential, see Fig.

S11 of [32]. We note that such a phenomenon resembles the interplay between single-particle excitations and photon-assisted tunneling occurring in superconducting junctions. Depending on the geometry the collective excitations can be different. For instance, in the theoretical proposal [12], a larger 2D system was used and vortex-antivortex pairs are generated instead of solitons. In earlier studies of the dissipation at an atomic Josephson junction, the creation of vortex ring excitations at the barrier was observed [37, 38].

DISCUSSION AND OUTLOOK

We have experimentally demonstrated the emergence of Shapiro steps in an ultracold quantum gas by emulating the external microwave field and an alternating particle current across the barrier with a periodic modulation of the barrier position. Exploiting the know-how of the cold atoms field, we could monitor the coherent dynamics of the system with unprecedented accuracy. This way, our work opens up new directions both in basic and applied physical science. On the fundamental side, different dimensions, geometries, and particle statistics are

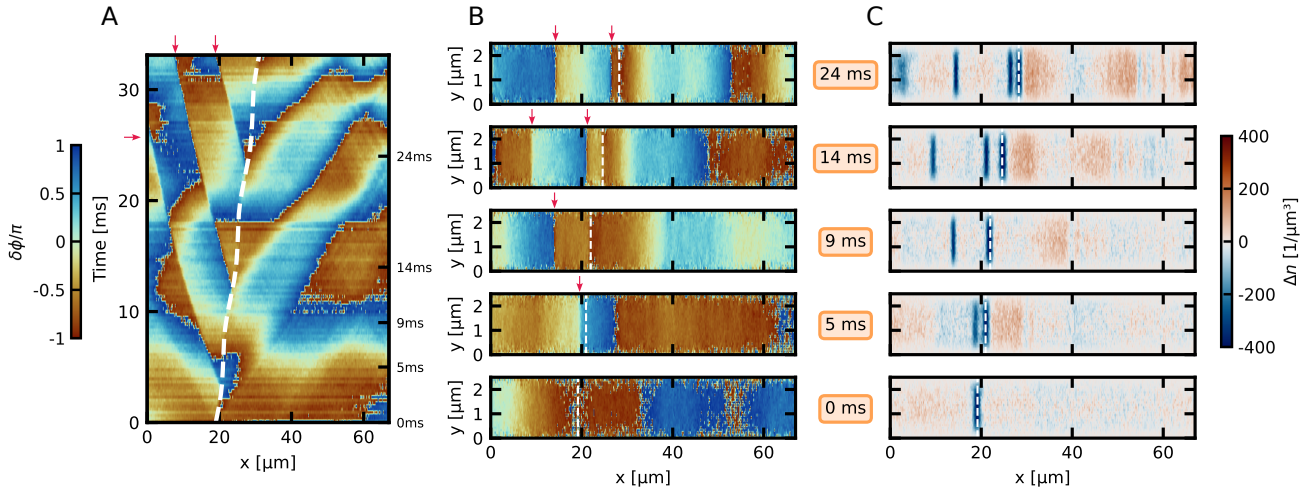


FIG. 4. **Soliton dynamics.** (A) Time evolution of the phase $\delta\phi(x)$ along the central x line of a single trajectory of the system for $I/I_c = 0.9$, $I_m/I_c = 0.8$ and $f_m = 90$ Hz. The periodic barrier motion (white dashed line) modifies the local phase near the barrier, which results in the creation of solitons moving to the left. The red arrows in (A) and (B) are a guide to the eye for the localization of the solitons. (B) Snapshots of the phase profile $\delta\phi(x, y)$ of a single trajectory and (C) the averaged density profile $\Delta n(x, y)$ for the central z plane at times $t = 0, 5, 9, 14$, and 24 ms. During each driving cycle the barrier motion (white vertical dashed line) emits one soliton of uniform phase along the y direction, which appear as density dips in (C). There are also phononic excitations that propagate in both forward and backward directions. In (C) we show the relative change of the density with respect to a reference cloud without barrier.

direct extensions, as well as superfluid mixtures, dipolar superfluids, and superfluids in optical lattices, which can give rise to new physical processes, e.g. by generating other types of solitons, such as bright solitons, or vortices, or defects related to an underlying lattice or competing orders. Indeed, Eq. 2 provides the possibility to measure the equation of state of strongly correlated many-body systems. In the context of superconducting Josephson junctions, our work motivates to expand the understanding of the microscopic dynamics of the Shapiro effect as well, including the role of superconducting quasi-particles, solitons and vortices.

On the application side, we remark that our system transfers the voltage standard to the field of ultracold quantum gases. Towards the development of atomtronic technology, Shapiro steps can be used to fine tune quantum transport, as they combine both superfluid and resistive transport. Stacks of Shapiro steps can be used to create even larger differences in chemical potential over a whole system, or as a source for predetermined chemical potential differences. We note that Shapiro steps have also been observed recently in an experiment with strongly correlated ultracold fermions in the unitary regime [39].

ACKNOWLEDGMENTS

We thank Giacomo Roati and Giulia Del Pace for useful discussions. **Funding:** We gratefully acknowledge financial support by the DFG within the SFB OSCAR (project number 277625399). L.M. acknowledges support by the Deutsche Forschungsgemeinschaft (DFG, German Research Foundation), namely the Cluster of Excellence ‘Advanced Imaging of Matter’ (EXC 2056), Project No. 390715994. The project is co-financed by ERDF of the European Union and by ‘Fonds of the Hamburg Ministry of Science, Research, Equalities and Districts (BWFGB)’. **Author contributions:** E.B., M.R. and H.O. conceived the study. E.B. and M.R. performed the experiment and analyzed the data. E.B. performed the GPE simulations and V.P.S. modeled classical-field simulations. H.O. supervised the experiment. L.M. and L.A. supervised the theoretical part of the project. E.B. prepared the initial version of the manuscript. All authors contributed to the data interpretation and the writing of the manuscript. **Competing interests:** The authors declare no competing interests. **Data and materials availability:** All data presented in this paper will be deposited at Zenodo.

* luigi.amico@tii.ae

[†] ott@physik.uni-kl.de

[1] B. Josephson, Possible new effects in superconductive tunnelling, *Physics Letters* **1**, 251 (1962).

[2] M. Tinkham, *Introduction to superconductivity*, Vol. 1 (Courier Corporation, 2004).

[3] R. L. Fagaly, Superconducting quantum interference device instruments and applications, *Review of Scientific Instruments* **77**, 101101 (2006), https://pubs.aip.org/aip/rsi/article-pdf/doi/10.1063/1.2354545/11171638/101101_1.online.pdf.

[4] D. Koelle, R. Kleiner, F. Ludwig, E. Dantsker, and J. Clarke, High-transition-temperature superconducting quantum interference devices, *Rev. Mod. Phys.* **71**, 631 (1999).

[5] A. Barone and G. Paterno, Physics and applications of the josephson effect (1982).

[6] A. J. Leggett, Macroscopic quantum tunnelling and related matters, *Japanese Journal of Applied Physics* **26**, 1986 (1987).

[7] J. Clarke and F. K. Wilhelm, Superconducting quantum bits, *Nature* **453**, 1031 (2008).

[8] J. Koch, T. M. Yu, J. Gambetta, A. A. Houck, D. I. Schuster, J. Majer, A. Blais, M. H. Devoret, S. M. Girvin, and R. J. Schoelkopf, Charge-insensitive qubit design derived from the cooper pair box, *Phys. Rev. A* **76**, 042319 (2007).

[9] M. W. Johnson, M. H. S. Amin, S. Gildert, T. Lanting, F. Hamze, N. Dickson, R. Harris, A. J. Berkley, J. Johansson, P. Bunyk, E. M. Chapple, C. Enderud, J. P. Hilton, K. Karimi, E. Ladizinsky, N. Ladizinsky, T. Oh, I. Perminov, C. Rich, M. C. Thom, E. Tolkacheva, C. J. S. Truncik, S. Uchaikin, J. Wang, B. Wilson, and G. Rose, Quantum annealing with manufactured spins, *Nature* **473**, 194 (2011).

[10] F. Arute, K. Arya, R. Babbush, D. Bacon, J. C. Bardin, R. Barends, R. Biswas, S. Boixo, F. G. S. L. Brandao, D. A. Buell, B. Burkett, Y. Chen, Z. Chen, B. Chiaro, R. Collins, W. Courtney, A. Dunsworth, E. Farhi, B. Foxen, A. Fowler, C. Gidney, M. Giustina, R. Graff, K. Guerin, S. Habegger, M. P. Harrigan, M. J. Hartmann, A. Ho, M. Hoffmann, T. Huang, T. S. Humble, S. V. Isakov, E. Jeffrey, Z. Jiang, D. Kafri, K. Kechedzhi, J. Kelly, P. V. Klimov, S. Knysh, A. Korotkov, F. Kostritsa, D. Landhuis, M. Lindmark, E. Lucero, D. Lyakh, S. Mandrà, J. R. McClean, M. McEwen, A. Megrant, X. Mi, K. Michielsen, M. Mohseni, J. Mutus, O. Naaman, M. Neeley, C. Neill, M. Y. Niu, E. Ostby, A. Petukhov, J. C. Platt, C. Quintana, E. G. Rieffel, P. Roushan, N. C. Rubin, D. Sank, K. J. Satzinger, V. Smelyanskiy, K. J. Sung, M. D. Tervithick, A. Vainsencher, B. Villalonga, T. White, Z. J. Yao, P. Yeh, A. Zalcman, H. Neven, and J. M. Martinis, Quantum supremacy using a programmable superconducting processor, *Nature* **574**, 505 (2019).

[11] S. Shapiro, Josephson currents in superconducting tunneling: The effect of microwaves and other observations, *Phys. Rev. Lett.* **11**, 80 (1963).

[12] R. Pöpel, The josephson effect and voltage standards, *Metrologia* **29**, 153 (1992).

[13] R. W. Simmonds, A. Marchenkov, J. C. Davis, and R. E. Packard, Observation of the superfluid shapiro effect in a ^3He weak link, *Phys. Rev. Lett.* **87**, 035301 (2001).

[14] M. Albiez, R. Gati, J. Fölling, S. Hunsmann, M. Cristiani, and M. K. Oberthaler, Direct observation of tunneling and nonlinear self-trapping in a single bosonic josephson junction, *Phys. Rev. Lett.* **95**, 010402 (2005).

[15] C. Ryu, P. W. Blackburn, A. A. Blinova, and M. G. Boshier, Experimental realization of josephson junctions for an atom squid, *Phys. Rev. Lett.* **111**, 205301 (2013).

[16] L. Amico, M. Boshier, G. Birk, A. Minguzzi, C. Miniatura, L.-C. Kwek, D. Aghamalyan, V. Ahufinger, D. Anderson, N. Andrei, A. S. Arnold, M. Baker, T. A. Bell, T. Bland, J. P. Brantut, D. Cassetta, W. J. Chetcuti, F. Chevy, R. Citro, S. De Palo, R. Dumke, M. Edwards, R. Folman, J. Fortagh, S. A. Gardiner, B. M. Garraway, G. Gauthier, A. Günther, T. Haug, C. Hufnagel, M. Keil, P. Ireland, M. Lebrat, W. Li, L. Longchambon, J. Mompart, O. Morsch, P. Naldesi, T. W. Neely, M. Olshanii, E. Orignac, S. Pandey, A. Pérez-Obiol, H. Perrin, L. Piroli, J. Polo, A. L. Pritchard, N. P. Proukakis, C. Rylands, H. Rubinsztein-Dunlop, F. Scazza, S. Stringari, F. Tosto, A. Trombettoni, N. Victorin, W. v. Klitzing, D. Wilkowski, K. Xhani, and A. Yakimenko, Roadmap on Atomtronics: State of the art and perspective, *AVS Quantum Science* **3**, 039201 (2021), https://pubs.aip.org/avs/aqs/article-pdf/doi/10.1116/5.0026178/19676772/039201_1.5.0026178.pdf.

[17] L. Amico, D. Anderson, M. Boshier, J.-P. Brantut, L.-C. Kwek, A. Minguzzi, and W. von Klitzing, Colloquium: Atomtronic circuits: From many-body physics to quantum technologies, *Rev. Mod. Phys.* **94**, 041001 (2022).

[18] S. Giovanazzi, A. Smerzi, and S. Fantoni, Josephson effects in dilute bose-einstein condensates, *Phys. Rev. Lett.* **84**, 4521 (2000).

[4] F. Meier and W. Zwerger, Josephson tunneling between weakly interacting bose-einstein condensates, *Phys. Rev. A* **64**, 033610 (2001).

[20] V. P. Singh, N. Luick, L. Sobirey, and L. Mathey, Josephson junction dynamics in a two-dimensional ultracold bose gas, *Phys. Rev. Res.* **2**, 033298 (2020).

[21] A. K. Saha and R. Dubessy, Dynamical phase diagram of a one-dimensional bose gas in a box with a tunable weak link: From bose-josephson oscillations to shock waves, *Phys. Rev. A* **104**, 023316 (2021).

[22] J. Grond, T. Betz, U. Hohenester, N. J. Mauser, J. Schmiedmayer, and T. Schumm, The shapiro effect in atomchip-based bosonic josephson junctions, *New Journal of Physics* **13**, 065026 (2011).

[23] L. J. LeBlanc, A. B. Bardon, J. McKeever, M. H. T. Extavour, D. Jervis, J. H. Thywissen, F. Piazza, and A. Smerzi, Dynamics of a tunable superfluid junction, *Phys. Rev. Lett.* **106**, 025302 (2011).

[24] S. Eckel, J. G. Lee, F. Jendrzejewski, C. J. Lobb, G. K. Campbell, and W. T. Hill, Contact resistance and phase slips in mesoscopic superfluid-atom transport, *Phys. Rev. A* **93**, 063619 (2016).

[25] S.-C. Ji, T. Schweigler, M. Tajik, F. Cataldini, J. a. Sabino, F. S. Møller, S. Erne, and J. Schmiedmayer, Floquet engineering a bosonic josephson junction, *Phys. Rev. Lett.* **129**, 080402 (2022).

[5] G. Valtolina, A. Burchianti, A. Amico, E. Neri, K. Xhani, J. A. Seman, A. Trombettoni, A. Smerzi, M. Zaccanti, M. Inguscio, and G. Roati, Josephson effect in fermionic superfluids across the bec-bcs crossover, *Science* **350**, 1505 (2015), <https://www.science.org/doi/pdf/10.1126/science.aac9725>.

[27] N. Luick, L. Sobirey, M. Bohlen, V. P. Singh, L. Mathey, T. Lompe, and H. Moritz, An

ideal josephson junction in an ultracold two-dimensional fermi gas, *Science* **369**, 89 (2020), <https://www.science.org/doi/pdf/10.1126/science.aaz2342>.

[2] W. J. Kwon, G. D. Pace, R. Panza, M. Inguscio, W. Zwerger, M. Zaccanti, F. Scazza, and G. Roati, Strongly correlated superfluid order parameters from dc josephson supercurrents, *Science* **369**, 84 (2020), <https://www.science.org/doi/pdf/10.1126/science.aaz2463>.

[29] G. Del Pace, W. J. Kwon, M. Zaccanti, G. Roati, and F. Scazza, Tunneling transport of unitary fermions across the superfluid transition, *Phys. Rev. Lett.* **126**, 055301 (2021).

[12] V. P. Singh, J. Polo, L. Mathey, and L. Amico, Shapiro Steps in Driven Atomic Josephson Junctions, *Phys. Rev. Lett.* **133**, 093401 (2024).

[3] L. Asteria, H. P. Zahn, M. N. Kosch, K. Sengstock, and C. Weitenberg, Quantum gas magnifier for sub-lattice-resolved imaging of 3d quantum systems, *Nature* **599**, 571 (2021).

[32] See supplementary.

[33] A. H. Dayem and R. J. Martin, Quantum interaction of microwave radiation with tunneling between superconductors, *Phys. Rev. Lett.* **8**, 246 (1962).

[34] C. A. Hamilton, Frequency dependence of the josephson current, *Phys. Rev. B* **5**, 912 (1972).

[35] C. A. Hamilton, Josephson voltage standards, *Review of Scientific Instruments* **71**, 3611 (2000), https://pubs.aip.org/aip/rsi/article-pdf/71/10/3611/19100354/3611_1.online.pdf.

[36] C. A. Hamilton and S. Shapiro, Experimental demonstration of the riedel peak, *Phys. Rev. Lett.* **26**, 426 (1971).

[37] A. Burchianti, F. Scazza, A. Amico, G. Valtolina, J. A. Seman, C. Fort, M. Zaccanti, M. Inguscio, and G. Roati, Connecting dissipation and phase slips in a josephson junction between fermionic superfluids, *Phys. Rev. Lett.* **120**, 025302 (2018).

[38] K. Xhani, E. Neri, L. Galantucci, F. Scazza, A. Burchianti, K.-L. Lee, C. F. Barenghi, A. Trombettini, M. Inguscio, M. Zaccanti, G. Roati, and N. P. Proukakis, Critical transport and vortex dynamics in a thin atomic josephson junction, *Phys. Rev. Lett.* **124**, 045301 (2020).

[39] G. Del Pace, D. Hernández-Rajkov, V. Singh, N. Grani, M. Frómeta Fernández, G. Nesti, J. Seman, M. Inguscio, L. Amico, and G. Roati, Shapiro steps in strongly-interacting fermi gases (2024), to be published.

SUPPLEMENTARY MATERIAL

EXPERIMENTAL DETAILS

Experimental procedure

We start by preparing a Bose-Einstein condensate (BEC) of around 180×10^3 ^{87}Rb atoms in a crossed optical dipole trap, consisting of a *High Power* (HP) beam and a *Low Power* (LP) beam. To reach the required tube like geometry we ramp the HP linearly in 400 ms from 20 mW up to 150 mW and the LP within the same time down to 0 mW. This results in a trapping geometry with trapping frequencies $\omega = 2\pi \times [1.6; 252; 250]$ Hz. Because the atoms can expand in the dipole trap during this procedure and to set a defined length of the sample we use two repulsive barriers at positions $x = \pm 37.5 \mu\text{m}$ from the center of the initial position of the BEC. The barriers are ramped linearly within 40 ms up to a intensity resulting in a potential much higher than the chemical potential of the cloud ($\approx 10\mu$).

When the ramp of the dipole trap is finished we wait 200 ms, letting the system equilibrate, before starting the experiment. After this wait time we ramp up the center barrier in 45 ms to its intended value with an initial position which is $20 \mu\text{m}$ off center. Subsequently, the Shapiro protocol starts, see main text.

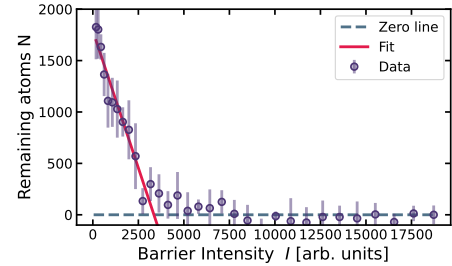
Barrier generation

The realization of the optical barriers are sketched in the following. We use a 532 nm laser to create a repulsive potential and an AOM to stabilize its intensity. To generate the barriers we guide the beam through a two axis acousto-optical deflector (AOD). By changing the AODs RF driving frequency we control the axial position and the transverse extent of the barriers. After the AOD we use a $f = 100$ mm scan lens to convert the beams angular displacement in a lateral displacement. The light is then collected by a $f = 750$ mm tube lens and guided to the NA = 0.3 in-vacuum objective, which focus the beam down to the atoms. The tube lens is chosen in a way that we get a diffraction limited spot at the atoms. We estimate the size of a single spot by a measurement with a test target in the chamber. The Gaussian beam radius is round $1.1 \mu\text{m}$.

To realize in the transverse direction a homogeneously extended and in the axial direction movable barrier, we drive the AOD by multiple RF frequencies [1]. By applying a multitone RF signal of the form

$$S(t) = \sum_i S_i \sin(\omega_i t + \phi_i), \quad (4)$$

to each of the AOD axis, we create three individual barriers, which are independently movable, when using time



Supplementary Figure 1. **Calibration of the barrier height.** A barrier block of 5×8 spots is projected into the center of the BEC. The atom number in the block area is measured and plotted against the barrier intensity. The solid line is a linear fit, according to $n = \mu/g$. The intersection with the abscissa defines the light intensity, for which $V_0 = \mu$

dependent $\phi_i(t)$. For the experiments described in the main text we use 40 mW laser power in total.

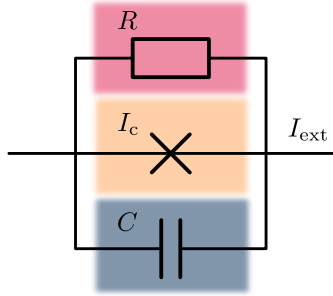
Calibration of the barrier height

To estimate the height of the barrier used in the experiment we measure the equation of state $n(\mu)$. The method is close to the one used in [2]. We generate a block of 5×9 barrier spots, which corresponds to 5 times the experiments barrier size and measure their mean intensity separately on a camera. This barrier block is projected onto the center of the BEC consisting of 180×10^3 atoms. We count the atoms at the position of the block by absorption imaging in the y-direction, applying the matter wave imaging scheme. The result is shown in fig. S1. The initial decrease is linearly fitted and the zero crossing is set as the barrier height corresponding to the chemical potential $V_0 = \mu$.

Imaging system

The atom cloud is probed via absorption imaging, using the 780 nm Rubidium D2 transition. Our experiment uses three different imaging systems. First we have a standard time of flight imaging along the y-axis (horizontal direction) with a magnification of $M_{\text{hor}} = 3.77$, which is used to measure the atom number of the BEC. Second we use the same imaging setup in a different mode, known as matter wave imaging [3]. This procedure enables us to image the density distribution of the cloud in position space after a certain time of flight with a magnification in the axial direction of $M_{\text{mwi}} = M'_{\text{mwi}} \cdot M_{\text{hor}} = 32.8$, were $M'_{\text{mwi}} = 8.7$. The benefit of the matter wave imaging system is a strongly reduced optical density, which allows for a precise atom number determination.

Last, we can perform *in-situ* absorption imaging through the NA = 0.3 objective along the z-axis (ver-



Supplementary Figure 2. **RCSJ circuit.** RCSJ model circuit to describe a Josephson junction.

tical direction). With this imaging scheme we can get a theoretical optical resolution of $d_{\text{vert}} = 1.6 \mu\text{m}$ and a magnification of $M_{\text{vert}} = 19.5$. However, the high optical density of the sample in the trap prevents us from correctly determining the density with *in-situ* imaging.

CHARACTERIZATION OF THE WEAK LINK

To effectively describe a Josephson junction in the un-driven case, one usually applies the so-called *resistively capacitively shunted junction* (RCSJ) model. There, an additional resistance R and capacity C is assigned to the junction and a simple circuit, see fig. S2, is used to quantitatively model the junctions behaviour. With Kirchoff's law we get the basic equation of the circuit

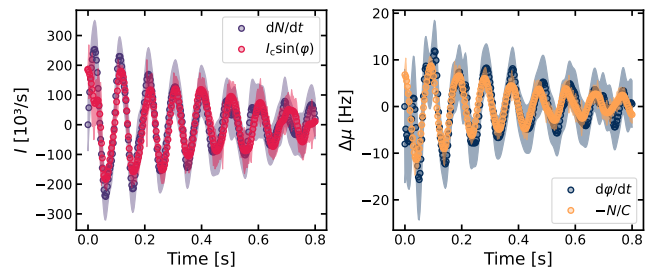
$$I_{\text{ext}} = I_c \sin(\phi) - \frac{1}{R} \Delta\mu - C \Delta\dot{\mu}. \quad (5)$$

Here, the first Josephson equation $I(\phi) = I_c \sin(\phi)$ is used to describe the supercurrent across the junction. In case of ultracold atoms, where the chemical potential difference $\Delta\mu$ plays the role of the voltage, the second Josephson equation reads [4]

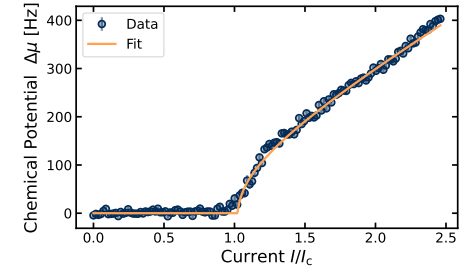
$$\Delta\mu = -\hbar \dot{\phi}. \quad (6)$$

To be able to fully describe the junction we use these equations to experimentally determine the systems parameters R , C , and I_c .

To this end, we measure Josephson plasma oscillations [5]. We first prepare an initial atom number imbalance across the junction and let the system evolve freely in time. We then measure both, the atom number difference $N = N_L - N_R$ and the relative phase $\phi = \phi_L - \phi_R$ between the two superfluids. Applying a Gaussian filter to the experimental data and numerical differentiation of N gives $\frac{dN}{dt}$, and by fitting I_c to $I(t) = \frac{dN}{dt} = I_c \sin(\phi(t))$ (see fig. S3), we find $I_c = 192 \times 10^3 \text{ 1/s}$. In the same way, we can determine the capacity C . Using the same measurement, we numerically differentiate $\phi(t)$ and together with Eq. 6 we get $-V(t) = -\frac{N(t)}{C} = \frac{d\phi}{dt}$. We find $C = 59.6 \text{ s/h}$.



Supplementary Figure 3. **Determination of the system parameters I_c and C .** We measure the atom number difference N and the relative phase ϕ of a Josephson plasma oscillation. Numerically differentiating N and ϕ and subsequently fitting I_c and C to the equations $\frac{dN}{dt} = I_c \sin(\phi(t))$, $\frac{d\phi}{dt} = -\frac{N}{C}$, gives to $I_c = 192 \times 10^3 \text{ 1/s}$ and $C = 59.6 \text{ s/h}$.

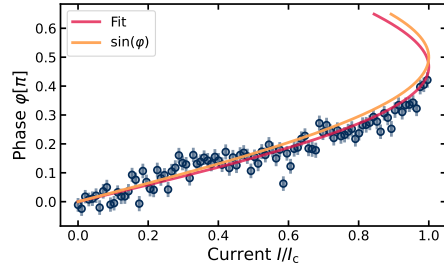


Supplementary Figure 4. **Determination of the resistance R .** Critical velocity measurement with fit to get the resistance $R = 0.9 \times 10^{-3} \text{ h}$.

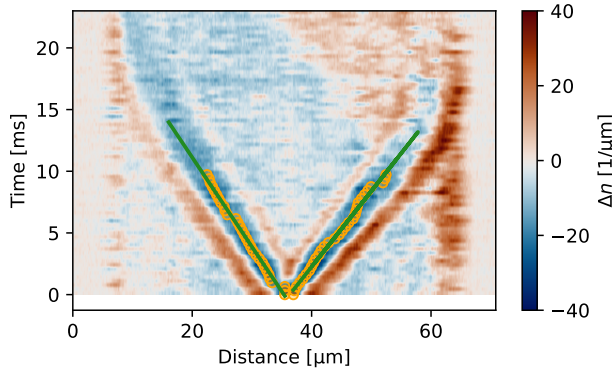
The resistance R can be determined by measuring the BEC critical velocity v_c . Thereby, we run a dc Josephson protocol, by moving the barrier with constant velocity through the condensate. The result is shown in fig. S4. Below the critical velocity v_c , we find $\Delta\mu = 0$, indicating the absence of any "voltage" drop. Above v_c , a finite chemical potential difference $\Delta\mu$ builds up, signaling the onset of the ac Josephson branch. Fitting $\Delta z = R \sqrt{v^2 - v_c^2}$, gives $v_c = 0.42 \text{ mm/s}$. With $I = v \cdot I_c / v_c$ and Eq. 7 we can rescale the measurement data and use again the fit function $\Delta\mu = R \sqrt{I^2 - I_c^2}$, and obtain $R = 0.9 \times 10^{-3} \text{ h}$.

Current phase relation

The Josephson junction in our experiments has a barrier height which is significantly lower than the chemical potential. It is necessary to independently measure the current phase relation in order to verify, whether higher order terms in the Josephson relation are relevant [6]. We repeat the experiment for the critical velocity and measure the phase between the two condensates at the end of the motion. The phase is determined via interference of both condensates in time of flight. We find the best



Supplementary Figure 5. **Current-phase relation of the Josephson junction.** Measurement of the current-phase relation of the Josephson junction using the dc Josephson effect. The phase difference across the barrier is plotted against the dc current. The yellow curve represents the ideal current phase-relation $I = I_c \sin(\varphi)$. The red curve is a fit including the second order term (see text).



Supplementary Figure 6. **Speed of sound measurement.** Ramp the barrier up to excite a density wave moving through the condensate and take absorption images to extract the velocity. For the wave of the right side $c_s = 1.63(3)$ mm/s and on the left side $c_s = -1.38(2)$ mm/s

contrast for 5 ms time of flight, for which a substantial part of the cloud has already interfered with each other. After subtracting a reference image without barrier we fit a sinusoidal function to extract the phase. The resulting current phase relation is shown in fig. S5. Following Ref. [4] one can describe the current phase relation of a Josephson junction with $I(\varphi) = \sum_{n>0} I_n \sin(n\varphi)$ if the system exhibits time reversal symmetry. In the limit of small coupling the above expression reduces to the first Josephson equation, $I(\varphi) = I_c \sin(\varphi)$. We fit our data up to the second order term and find $I_1 = 0.995 I_c$ and $I_2 = 0.054 I_c$. The Josephson junction is therefore close to the ideal Josephson junction limit.

Speed of sound

We measure the speed of sound following the original protocol from Ref. [7]. We prepare the same sample as in

the Shapiro step measurements. We then instantaneously switch on a barrier with height $V_B \approx \mu$ in the center of the condensate. We follow the resulting phonon propagation via matter wave imaging, subtracting a reference image without barrier (see fig. S6). We extract from a linear fit the speed of sound. The density wave traveling to the right has a speed of $c_s = 1.63(3)$ mm/s, and the one traveling to the left has a speed of $c_s = -1.38(2)$ mm/s. The small difference probably rises from a residual motion of the condensate in the shallow trap.

Shapiro steps for different barrier height

To see the influence of the barrier height on the occurrence of the Shapiro steps, we repeat the same protocol for a large range of different barrier heights as shown in fig. S7. Shapiro steps are visible over the whole parameter range. However, the steps tend to smear out for very high barriers (corresponding to a smaller critical current), while for lowest barrier height ($V_B = 0.25\mu$), the step height is reduced. We attribute the latter to the fact that the “weak link regime” is no longer valid for such low barriers.

MEASUREMENT EVALUATION

Chemical potential

To map the measured atom number differences Δz to a chemical potential difference $\Delta\mu$, we calculate μ for different total atom numbers N , see fig. S8, using imaginary time evolution of the GPE [8]. We then extract the chemical potential from the calculated ground state wave function, and use a phenomenological fit to get a function $\mu(N)$. With

$$\Delta\mu(z) = \mu(N \cdot (1+z)) - \mu(N \cdot (1-z)) \quad (7)$$

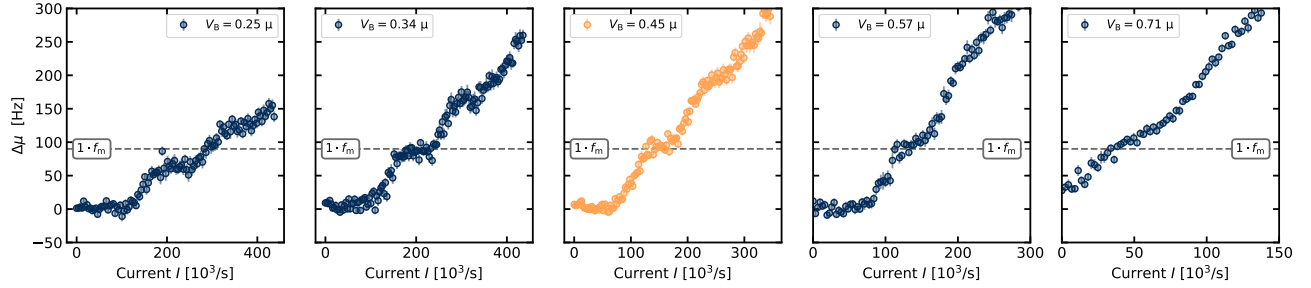
we calculate $\Delta\mu(z)$.

Step height

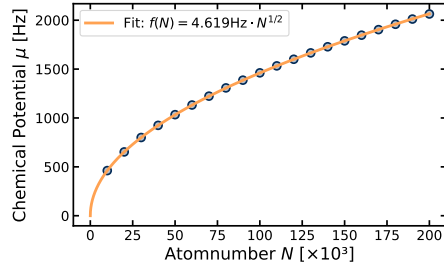
To evaluate the step height, we rescale the data to chemical potential differences using Eq. 7 and fit a logistic function

$$f(x) = \sum_i \frac{S}{1 + \exp(-k_i(x - x_i))} + b, \quad (8)$$

where S is the step height, k_i the steepness of the steps and $i-1$ the number of visible steps.



Supplementary Figure 7. **Shapiro steps for different barrier heights.** Barrier heights between 0.25μ and 0.7μ for a modulation frequency of $f_m = 90$ Hz. The steps are clearly visible over the complete parameter range. However, deviations start to be visible at the edges of the parameter range (see text).



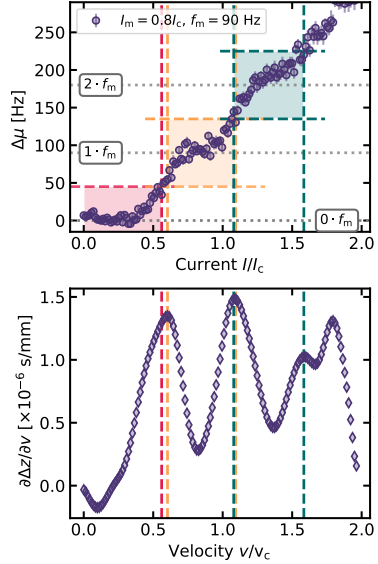
Supplementary Figure 8. **Chemical potential μ in dependence of the total atom number.** The calculation was done using imaginary time evolution of the Gross-Pitaevskii equation for the given system parameters.

Step width

We extract the width of the steps as illustrated in fig. S9. We first apply a Gaussian filter to the data to reduce high frequency noise before we numerically calculate the first derivative $\frac{\partial \Delta z}{\partial v}$ of the recorded atom number imbalance Δz . For each step n we search the maxima of the derivative in the area where $\Delta\mu = nf_m \pm \epsilon$, with $\epsilon = 45$ Hz. We define the width of a step I_n as the distance between the two maxima. For the 0-th step we calculate the distance with respect to zero. I_n is normalized by I_0 , which is the width of 0-th step in the dc Josephson protocol.

CLASSICAL-FIELD SIMULATION METHOD

We simulate the dynamics of a driven atomic Josephson junction using a classical-field method within the truncated Wigner approximation [9, 10]. We consider a three-dimensional (3D) condensate of ^{87}Rb atoms confined in a cigar-shaped geometry. The system is described



Supplementary Figure 9. **Illustration of the step width evaluation** **Upper:** Shapiro Step dataset where the shaded areas mark $\Delta\mu = nf_m \pm \epsilon$, with $\epsilon = 45$ Hz. **Lower:** First derivative of the Shapiro Step dataset, vertical lines mark the maxima of the derivative D_M in the area $\Delta\mu = nf_m \pm \epsilon$.

by the Hamiltonian

$$\hat{H} = \int d\mathbf{r} \left[\frac{\hbar^2}{2m} \nabla \hat{\psi}^\dagger(\mathbf{r}) \cdot \nabla \hat{\psi}(\mathbf{r}) + V(\mathbf{r}) \hat{\psi}^\dagger(\mathbf{r}) \hat{\psi}(\mathbf{r}) + \frac{g}{2} \hat{\psi}^\dagger(\mathbf{r}) \hat{\psi}^\dagger(\mathbf{r}) \hat{\psi}(\mathbf{r}) \hat{\psi}(\mathbf{r}) \right], \quad (9)$$

where $\hat{\psi}(\mathbf{r})$ and $\hat{\psi}^\dagger(\mathbf{r})$ are the bosonic annihilation and creation field operators, respectively. The 3D interaction parameter is given by $g = 4\pi a_s \hbar^2 / m$, where a_s is the s -wave scattering length and m is the mass. For ^{87}Rb atoms a_s is 5.3 nm. The external potential $V(\mathbf{r})$ represents the harmonic trap $V_{\text{trap}}(\mathbf{r}) = m(\omega_x^2 x^2 + \omega_y^2 y^2 + \omega_z^2 z^2)/2$, where the trap frequencies are chosen according to the experiment, i.e., $(\omega_x, \omega_y, \omega_z) = 2\pi \times (1.6, 252, 250)$ Hz. Within the classical-field approx-

imation we replace the operators $\hat{\psi}$ in Eq. 9 and in the equations of motion by complex numbers ψ . We map real space on a lattice system of $760 \times 25 \times 25$ sites with the lattice discretization length $l = 0.1 \mu\text{m}$. We note that the continuum limit is satisfied by choosing l to be comparable or smaller than the healing length $\xi = \hbar/\sqrt{2mgn}$ and the de Broglie wavelength, where n is the density [11]. We generate the initial states $\psi(t=0)$ in a grand canonical ensemble of temperature T and chemical potential μ via a classical Metropolis algorithm. We use $T = 35 \text{ nK}$ and adjust μ such that the total atom number N is close to the experimental one. We propagate each initial state using the classical equations of motion.

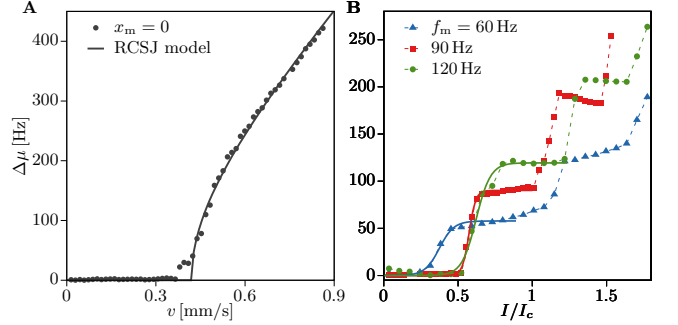
To create a Josephson junction and excite Shapiro steps we add a perturbation term $\mathcal{H}_{ex} = \int d\mathbf{r} V(x,t)n(\mathbf{r},t)$, where $n(\mathbf{r},t) = |\psi(\mathbf{r},t)|^2$ is the local density and $V(x,t)$ is the Gaussian barrier potential of the form

$$V(x,t) = V_0(t) \exp\left[-\frac{2(x - x_0 - x(t))^2}{w^2}\right]. \quad (10)$$

V_0 is the time-dependent strength and w is the width. x_0 is the initial location of the barrier and $x(t)$ is the dc and ac driving term. We choose $w = 1 \mu\text{m}$ and $x_0 = 19 \mu\text{m}$. We linearly ramp up $V_0(t)$ to the value $V_0/\mu = 0.45$ over 200 ms and then wait for 50 ms. This creates a weak link by suppressing the tunneling at location x_0 . While we move the barrier at a constant velocity v , we also periodically modulate its position as

$$x(t) = vt + x_m \sin(2\pi f_m t), \quad (11)$$

where x_m is the driving amplitude and f_m is the driving frequency [12]. This induces an atom current I relative to the barrier motion, i.e., $I = vI_c/v_c$, where I_c is the critical current and v_c is the critical velocity. Similarly, the amplitude of the ac current is given by $I_m = 2\pi f_m x_m I_c/v_c$. For the calculation of the atom imbalance we fix the driving time to 33 ms. The atom imbalance z is determined by $z = (N_R - N_L)/N$, where N_L (N_R) is the atom number in the left (right) reservoir, and $N = N_L + N_R$ is the total atom number. For various values of I , I_m , and f_m we determine $\Delta z = z - z_{\text{ref}}$ and convert it to the chemical potential difference $\Delta\mu$ using Eq. 7. z_{ref} is the imbalance determined at the final location without the ac driving the onset of a nonzero $\Delta\mu$ occurs above a certain v_c , which we determine using the prediction of the RCSJ circuit model, see Fig. 10 A. We obtain $v_c = 0.42 \text{ mm/s}$ in excellent agreement with the measurement of v_c . In the presence of ac drive we find the creation of Shapiro steps whose height depends on the driving frequency f_m . Using sigmoid fits we determine the height of the first Shapiro step, see Fig. 10 B. We determine the step height for f_m in the range between 50 and 185 Hz by analyzing the driven response after 3 to 6 driving periods, and also average these results over a few values of I_m . We determine the width



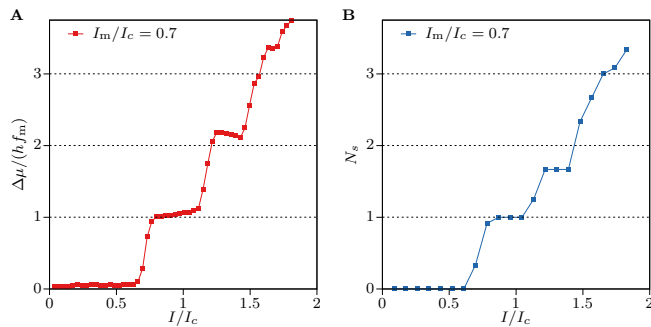
Supplementary Figure 10. **Simulation without and with ac driving.** (A) Simulated response after 33 ms as a function of the dc velocity v , which we fit with the result of the RCSJ circuit model: $\Delta\mu = R\sqrt{v^2 - v_c^2}$ using R and v_c as the fitting parameters. (B) Driven response as a function of the dc current I/I_c for the driving frequency $f_m = 60, 90$ and 120 Hz and the driving amplitude $I_m/I_c = 0.9$. The heights of the first step are determined using sigmoid fits (continuous lines).

of zeroth and first step following the same procedure as in the experiment, which involves calculating the differential resistance $d\Delta\mu/dI$ and then determining the step width from the maximum of $d\Delta\mu/dI$, see Fig. S9. The simulation results of the step width for $f_m = 90 \text{ Hz}$ and varying I_m/I_c are presented in the main text of the paper. For the phase evolution we calculate the local phase $\delta\phi(\mathbf{r}) = \phi(\mathbf{r}) - \phi(\mathbf{r}_{\text{ref}})$ from the time evolution of a single trajectory, where $\phi(\mathbf{r}_{\text{ref}})$ is the reference phase.

To count total number of solitons we analyze the phase evolution $\delta\phi(x,t) = \phi(x + l,t) - \phi(x,t)$ of a single line along the x direction of a single trajectory of the driven system, which is because the phase profile in the yz plane is almost uniform. The oscillating motion of the barrier results in the creation of solitons, which we identify by a phase jump of less than π . We count total number of such phase jumps to determine the soliton number N_s . In Fig. S11B we show N_s , averaged over few samples and total number of driving cycles, as a function of I/I_c , which features a step-like behavior, coinciding with the one observed in the $I - \Delta\mu$ characteristic in Fig. S11A. There are on-average one, two and three solitons at the first, second and third Shapiro steps, respectively.

SUPPLEMENTARY REFERENCES

- * luigi.amico@tii.ae
- † ott@physik.uni-kl.de
- [1] M. Endres, H. Bernien, A. Keesling, H. Levine, E. R. Anschuetz, A. Krajenbrink, C. Senko, V. Vuletic, M. Greiner, and M. D. Lukin, Atom-by-atom assembly of defect-free one-dimensional cold atom arrays, *Science* **354**, 1024 (2016), <https://www.science.org/doi/pdf/10.1126/science.aah3752>.
- [2] W. J. Kwon, G. D. Pace, R. Panza, M. Inguscio,



Supplementary Figure 11. **Shapiro step mechanism.** **(A)** Simulation result of the current-chemical potential characteristic for $f_m = 90$ Hz and $I_m/I_c = 0.7$. **(B)** Total number of solitons, N_s , created in the system for the same parameters as in A, which is determined after averaging over a few samples.

W. Zwerger, M. Zaccanti, F. Scazza, and G. Roati, Strongly correlated superfluid order parameters from dc josephson supercurrents, *Science* **369**, 84 (2020), <https://www.science.org/doi/pdf/10.1126/science.aaaz2463>.

- [3] L. Asteria, H. P. Zahn, M. N. Kosch, K. Sengstock, and C. Weitenberg, Quantum gas magnifier for sub-lattice-resolved imaging of 3d quantum systems, *Nature* **599**, 571 (2021).
- [4] F. Meier and W. Zwerger, Josephson tunneling between weakly interacting bose-einstein condensates, *Phys. Rev.*

A **64**, 033610 (2001).

- [5] G. Valtolina, A. Burchianti, A. Amico, E. Neri, K. Xhani, J. A. Seman, A. Trombettoni, A. Smerzi, M. Zaccanti, M. Inguscio, and G. Roati, Josephson effect in fermionic superfluids across the bec-bcs crossover, *Science* **350**, 1505 (2015), <https://www.science.org/doi/pdf/10.1126/science.aac9725>.
- [6] A. A. Golubov, M. Y. Kupriyanov, and E. Il'ichev, The current-phase relation in josephson junctions, *Rev. Mod. Phys.* **76**, 411 (2004).
- [7] M. R. Andrews, D. M. Kurn, H.-J. Miesner, D. S. Durfee, C. G. Townsend, S. Inouye, and W. Ketterle, Propagation of sound in a bose-einstein condensate, *Phys. Rev. Lett.* **79**, 553 (1997).
- [8] C. Baals, A. G. Moreno, J. Jiang, J. Benary, and H. Ott, Stability analysis and attractor dynamics of three-dimensional dark solitons with localized dissipation, *Phys. Rev. A* **103**, 043304 (2021).
- [9] V. P. Singh, W. Weimer, K. Morgener, J. Siegl, K. Hueck, N. Luick, H. Moritz, and L. Mathey, Probing superfluidity of Bose-Einstein condensates via laser stirring, *Phys. Rev. A* **93**, 023634 (2016).
- [10] H. Kiehn, V. P. Singh, and L. Mathey, Superfluidity of a laser-stirred Bose-Einstein condensate, *Phys. Rev. A* **105**, 043317 (2022).
- [11] C. Mora and Y. Castin, Extension of Bogoliubov theory to quasicondensates, *Phys. Rev. A* **67**, 053615 (2003).
- [12] V. P. Singh, J. Polo, L. Mathey, and L. Amico, Shapiro Steps in Driven Atomic Josephson Junctions, *Phys. Rev. Lett.* **133**, 093401 (2024).